Kinetic Effects on the Austenite Carbon Equivalent and Eutectic Carbon Equivalent of Silicon Cast Irons

Jacques Lacaze

Kinetic effects on the austenite carbon equivalent and eutectic carbon equivalent of silicon cast irons

Jacques LACAZE
CIRIMAT, Université de Toulouse, CS 44362, 31030 Toulouse, France

E-mail: Jacques.lacaze@ensiacet.fr

Abstract

The so-called carbon equivalent of austenite liquidus (CEL) and eutectic carbon equivalent (CE) that are used in cast iron metallurgy are known as linear functions of the composition. This paper first reminds how CEL and CE expressions are obtained from the knowledge of the relevant equilibrium phase diagram, emphasizing that they are not the same quantities. To account for the observed differences between these expressions and the experimental ones, it has been proposed in the literature to add kinetic terms to the equilibrium expressions. This is first discussed by considering austenite liquidus data for cast irons with 1 wt.% to 3 wt.% silicon, from which the appropriateness of the CEL is confirmed while also evidencing the role of austenite growth undercooling. Then, experimental results on the solidification onset of near eutectic (slightly hypo- and mildly hyper-eutectic) and strongly hyper-eutectic cast irons are considered for discussing the significance of CE. For this second part, alloys that solidify in the stable system were considered whose results show again the role of austenite growth undercooling, but also that of graphite growth undercooling. The effects of addition of magnesium and of inoculation are discussed.

Keywords: cast iron, thermal analysis, austenite carbon equivalent, eutectic carbon equivalent

Competing Interests: The author declares no competing interest.

Introduction

Thermal analysis of silicon cast irons refers to two quantities, the carbon equivalent of austenite liquidus (CEL) and the carbon equivalent (CE). The CEL –also called austenite carbon equivalent, ACE [1]- is directly related to the austenite liquidus while the CE is used to locate the alloys with respect to the stable eutectic. In foundry practice of usual silicon cast irons with less than 3 wt.% Si, these two quantities are expressed as a first order (linear) polynomial of the composition whose coefficients differ as noticed long ago, e.g. by Moore [2, 3]. Because the solidification of melts deviates from equilibrium, Lekakh [4] pointed out that the experimental CE expression could contain terms describing kinetic effects, and this conclusion must apply to the CEL. Such a statement means that the body of the expressions for CEL and CE should come from the description of the equilibrium phase diagram, and that the kinetic effects should appear as additions to these equilibrium expressions [4].

Stefanescu recently proposed to analyze the effect of magnesium on CE using data from literature giving the temperature for solidification onset [5]. The present work uses part of this database and adds other references to successively analyze thermal analysis results on austenite liquidus in relation to CEL and on graphite liquidus in relation to CE, with a particular focus on near-eutectic alloys. This approach illustrates further a previous evaluation of thermal analysis of silicon cast irons [6] and begins with a reminder of the CEL and CE equilibrium expressions.

Equilibrium CEL and CE values

Basically, a linear expression for the CEL is based on the assumption that the austenite liquidus can be described as a plane in the appropriate phase diagram, although this may only be valid for a limited compositional range. For the usual silicon melts that are alloys based on the Fe-C-Si system with a silicon content of less than 3 wt.%, the austenite and graphite liquidus have effectively been described with good accuracy as planes [7, 8]. The effect of other elements (X) whose amount was limited to a maximum of 1 wt.% was also considered on the basis of the phase diagram information of Fe-C-X systems. Restricting to the elements relevant for the subsequent analysis, the equilibrium austenite liquidus, T_L^γ, and graphite liquidus, T_L^G, were expressed as follows:

$$T_L^\gamma = 1576.3 - 97.3 \cdot w_C - 23.0 \cdot w_{Si} - 4.08 \cdot w_{Cu} - 5.66 \cdot w_{Mn} \quad (1)$$

$$T_L^G = -534.7 + 389.1 \cdot w_C + 113.2 \cdot w_{Si} + 40.62 \cdot w_{Cu} - 2.40 \cdot w_{Mn} \quad (2)$$

where w_i is the content in i element (wt.%).

A comparison of calculations performed with Thermocalc's TCFE-8 database [9] and the above equations has been provided previously [10] and confirms the value of the above expressions.

Equation (1) can be written as:

$$T_L^{\gamma} = 1576.3 - 97.3 \cdot CEL_{99} \quad (3)$$

where the equilibrium carbon equivalent of austenite liquidus CEL is given by:

$$CEL_{99} = w_C + 0.236 \cdot w_{Si} + 0.042 \cdot w_{Cu} + 0.058 \cdot w_{Mn} \quad (4)$$

It may be noted that the silicon coefficient in CEL_{99} is in between the often mentioned values of 0.22 [1] and 0.25 [11]. It may be useful to note also that Moore [3] found an excellent fit with the silicon coefficient in his experimental CEL expression set at either 0.22 or 0.25; see later the description of Figure 1.

The eutectic line in the stable Fe-C-Si system is located at the intersection of the austenite and graphite liquidus. Equating equations (1) and (2), we obtained a first order equation relating the carbon and silicon contents along this line [7, 8]:

$$w_C^{eut} = w_C - 0.28 \cdot w_{Si} - 0.092 \cdot w_{Cu} - 0.007 \cdot w_{Mn} \quad (5)$$

This expression translates into the following definition of equilibrium CE:

$$CE_{99} = w_C + 0.28 \cdot w_{Si} + 0.092 \cdot w_{Cu} + 0.007 \cdot w_{Mn} \quad (6)$$

It is interesting to notice the difference between CE and CEL. Restricted to the silicon content, Eq. 4 and Eq. 6 give:

$$CE_{99} - CEL_{99} = 0.044 \cdot w_{Si} \quad (7)$$

which thus amounts to a non-negligible value that increases from 0.044 to 0.132 for cast irons with 1 wt.% Si to 3 wt.% Si. The whole point of the first-order approach detailed above is to demonstrate that CEL and CE should not be confused.

Finally, it is also worth mentioning that the eutectic temperature of the stable system, T_{EUT}, is obtained by inserting Equation 5 in Equation 1 (or Equation 2) and writes:

$$T_{EUT} = 1154.02 + 4.246 \cdot w_{Si} + 4.86 \cdot w_{Cu} - 5.00 \cdot w_{Mn} \qquad (8)$$

Selected data

For the analysis of the austenite liquidus data, a part of the database selected by Stefanescu [5] was considered to which some other results were added. In Stefanescu's database, the first set of data were from Chaudhari et al. [12] on base and Ni-Mg spheroidized melts. To the selection of results presented in Table 5 of Stefanescu's paper, a few more alloys were added and the entire set of results from Chaudhari et al. considered here is listed in Tables 1 and 2; see Appendix A. The data of Alonso et al. [13] were not considered because they are from the upper and lower regions of castings designed for thermal analysis simultaneously with coupled displacement measurements and showed wide variations in cooling rates at both positions that could explain the scatter observed when attempting to use these results. Then, the results of Anjos' thesis (Table 7 of Stefanescu's database) were included together with some other results of the same author [14]. Anjos' results all were on fully spheroidized alloys. In tables 8 and 10 of Stefanescu's database are listed the results of Regordosa et al. [8] and Ai et al. [15] dealing with partially spheroidized melts that were included in the present analysis. The increments in silicon content in Ai's results because of increased inoculation were taken from Stefanescu's table 10. The results in Table 9 of Stefanescu's paper are from 4 wt% Si melts that have been fully analyzed previously [16]; they were not considered in the present study due to the too high silicon content for which the linear equations presented above are not valid. Finally, the Dawson and Popelar results cited in Table 11 of Stefanescu's paper were also considered. Additional data of Moore [3] and Alagarsamy et al. [17] that have already been used in a previous report [18] have been considered here again. In summary, all selected data were from silicon cast irons with 1 to 3 wt.% silicon, cast in thermal analysis sand cups with the exception of the results from Dawson and Popelar that were obtained with the Sintercast steel cups.

Austenite liquidus data

The experimental austenite liquidus will be referred to as T_{LA} in the following. From the data set presented above, series were first selected that clearly included hypoeutectic alloys, i.e., excluding series with only T_{LA} values below the stable eutectic temperature. Such a selection will be made evident in the subsequent discussion. T_{LA} values are reported in Figure 1 as function of CEL_{99} calculated accounting for Cu and Mn content as appropriate. The solid line corresponds to the equilibrium austenite liquidus T_L^{γ} calculated with Equation (3). The

horizontal shaded area indicates the range of the eutectic equilibrium temperature according to equation (8), which varies from 1158.3°C at 1 wt.% Si to 1166.7°C at 3 wt.% Si.

In the range of CEL values of most interest, i.e., above 3.6 wt.%, the experimental values show a clear linear trend supporting the definition and use of this quantity. Moore's results for alloys with 1 wt.% Si and 3 wt.% Si represent a useful average of other data extending well below the stable eutectic through the use of Te-coated cups. Moore's results were therefore used to determine the following expression for T_{LA} by best fit:

$$T_{LA} = 1662 - 123.6 \cdot CEL_{99} \qquad (9)$$

In practice, correlations such as that given by Equation 9 could be established by foundries to account for their own melting process and to optimize their use of thermal analysis.

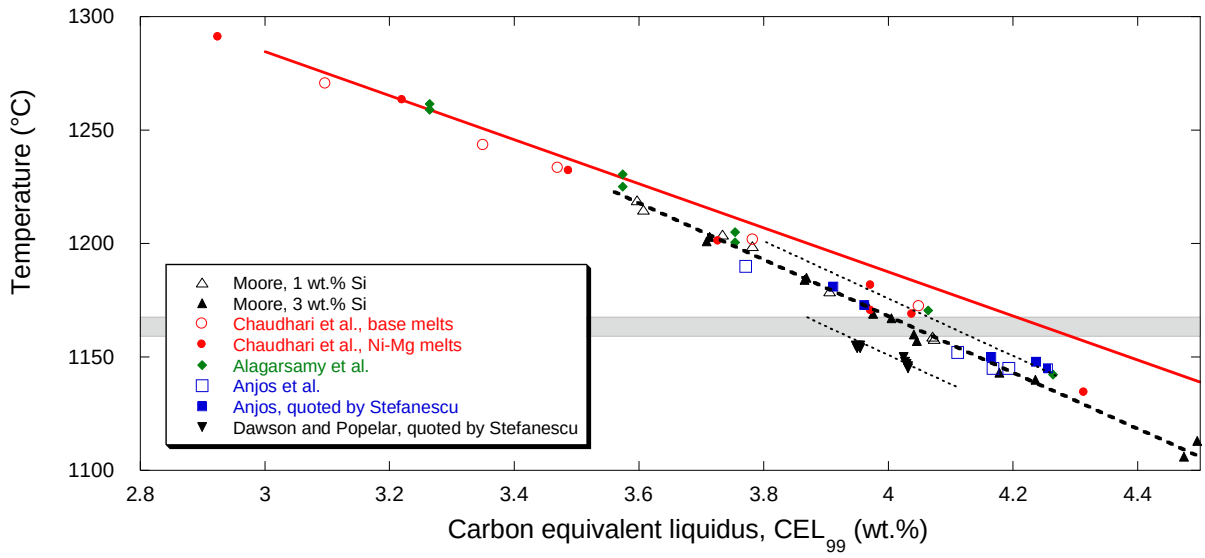

Figure 1. Symbols represent T_{LA} values from Moore [3], Chaudhari et al. [12], Alagarsamy et al. [17], Anjos et al. [14] and Anjos cited by Stefanescu [5], and Dawson and Popelar also quoted by Stefanescu. The solid line is the equilibrium austenite liquidus calculated with Equation (3), the bold dashed line is the best fit through Moore's data (equation 9) and the horizontal shaded area indicates the range of the eutectic equilibrium temperatures. The short dashed lines illustrate the effect of change in cooling rate due to differing thermal cups (see text).

Equation 9 has been plotted as a bold dashed line in Figure 1 for CEL_{99} values above 3.6 wt.%. For values of CEL around 4.0 wt.%, two dotted lines have also been drawn, one above

and the other below Equation 9. The line above goes through a couple of results from Alagasarmy et al. that were already noticed to show smaller undercooling with respect to the equilibrium austenite liquidus than Moore's results [18], probably because of the use of different cups. The line below goes through the results from Dawson and Propelar that show much higher undercooling because of a significantly higher cooling rate achieved in the steel cup of the Sintercast process. Therefore, there is a clear kinetic effect related to thermal transfer that could possibly be expressed as function of cooling rate.

It is noted that the difference between the equilibrium austenite liquidus and T_{LA} values increases with the CEL value, strongly suggesting that there is also an effect of carbon content. It has indeed been shown that the growth undercooling of austenite dendrite tips increases with carbon content [16] and strongly depends on the growth rate of the austenite dendrite front growing from the surface of the cup. However, it was noticed that the increase of undercooling due to carbon calculated at given growth rate could not explain the very large difference between T_L^{γ} and T_{LA} observed in Figure 1 at high CEL values unless it is assumed that the growth rate of the dendritic front increases with the carbon content. Though this is quite possible because the solidification temperature decreases with the carbon content, a better understanding of this phenomenon requires micro-macroscopic calculations. Such calculations have already been performed by Mampaey [19] but focusing on the austenite growth undercooling. This type of numerical approach, if extended to the eutectic transformation, would allow to solve the coupled effects of the temperature field and solidification kinetics in the thermal analysis cups [4].

To summarize, two kinetic effects affect the estimation of the austenite liquidus, one related to thermal transfer and the other due to carbon content and dependent as well of thermal transfer. A comparison of the experimental correlation such as equation (9) with the equilibrium one given by equation (3) suggests to write the kinetic carbon equivalent of austenite liquidus, CEL_{KIN}, as:

$$CEL_{KIN} = f(w_C, V_R) \cdot CEL_{99} \qquad (10)$$

where $f(w_C,V_R)$ is a function of the carbon content, w_C, and the cooling rate, V_R. In this equation, the cooling rate can be replaced by any quantity closely related to heat transfer, such as the thermal modulus or the solidification time.

Also, Mampaey [20] and Stefanescu [5] reminded that change in T_{LA} can be due to the oxidation state of the melt that is expected to depend on the melt processing and thus to be fairly reproducible in any foundry. For the present analysis, the effect of low-level elements such as Te and Mg on austenite liquidus should be considered. Moore [3] concluded that Te has no measurable effect on T_{LA} and Alagarsamy et al. [17] did not mention any effect either. It is therefore accepted that this element, added in low concentration, does not affect the austenite liquidus. Regarding Mg, it is interesting to note that Alonso et al. [13] performed a statistical analysis of their results that did not show a correlation between T_{LA} and Mg content thus confirming a previous statement by Frost and Stefanescu [21]. Similarly, Chaudhari et al. [12] and Mampaey [20] noted no effect of Mg on T_{LA}. The fact that there is no significant effect of magnesium on the equilibrium liquidus of austenite and graphite at the level where it is added for spheroidizing iron melts is further justified by thermodynamic calculations in Appendix B. Other works referenced by Stefanescu [5] to discuss the effect of Mg are those of Basutkar et al. [22], Yamane et al. [23], and Regordosa et al. [8], all of which involved hypereutectic alloys. Detailed data were not provided by Basutkar et al. so their results could not be considered here, while the results of Yamane et al. are mentioned in Appendix B. The results of Regordosa et al. appear in the following section.

Solidification onset of near-eutectic and hypereutectic silicon cast irons

The focus is now on the onset of solidification of near-eutectic- i.e., slightly hypo- to mildly hypereutectic- and strongly hyper-eutectic alloys with the eutectic reaction taking place in the stable system. Because of the change in eutectic temperature with silicon content, the CEL can no longer be used and so results must be reported as a function of carbon content or CE value, taking care to select data within a limited range of silicon contents [6]. From the data selection described above, we considered series of alloys including near-eutectic and hypereutectic compositions that were cast in plain cups (without tellurium). Considering the available data, alloys with silicon contents between 2.14 and 2.80 wt.% Si were selected, with an average of 2.45 wt.% Si which corresponds to the silicon content of the alloys studied by Regordosa et al. [8]. In this latter work, a spheroidized melt was maintained in a pressurized unit for hours, leading to a limited loss of carbon and silicon and a significant loss of magnesium. Every 30 minutes or so, two thermal analysis cups were poured, one empty and the other containing a given amount of inoculant. 19 castings were thus carried out.

These results are shown in Figure 2 where they have been reported as function of CE_{99} calculated with Equation 6 accounting for Cu and Mn when appropriate. In the figure, the solid lines represent the equilibrium diagram, with the austenite liquidus calculated with Equation 1 and extrapolated below the eutectic temperature, T_{EUT}, and the graphite liquidus calculated with Equation 2. For these latter calculations, the silicon content was set to 2.45 wt.% and no other alloying element was considered. The best-fit curve through Moore's data Equation 9 is reported with a short dashed line for the same silicon content of 2.45 wt.%.

In the area of highly hypereutectic alloys, the two dashed lines relate to the experimental liquidus arrest for lamellar (LG) and spheroidal (SG) graphite according to the results of Chaudhari et al. [12]. They reveal that primary graphite growth requires high undercooling (driving force) relative to the equilibrium liquidus of graphite, and that this undercooling is strongly dependent on the magnesium content [6, 16]. Another important feature of Figure 2 is that near-eutectic alloys, from slightly hypo-eutectic through mildly hyper-eutectic alloys, start solidifying in a narrow range of temperature. These two features are highlighted in Figure 3 that is a zoom of the central part of figure 2.

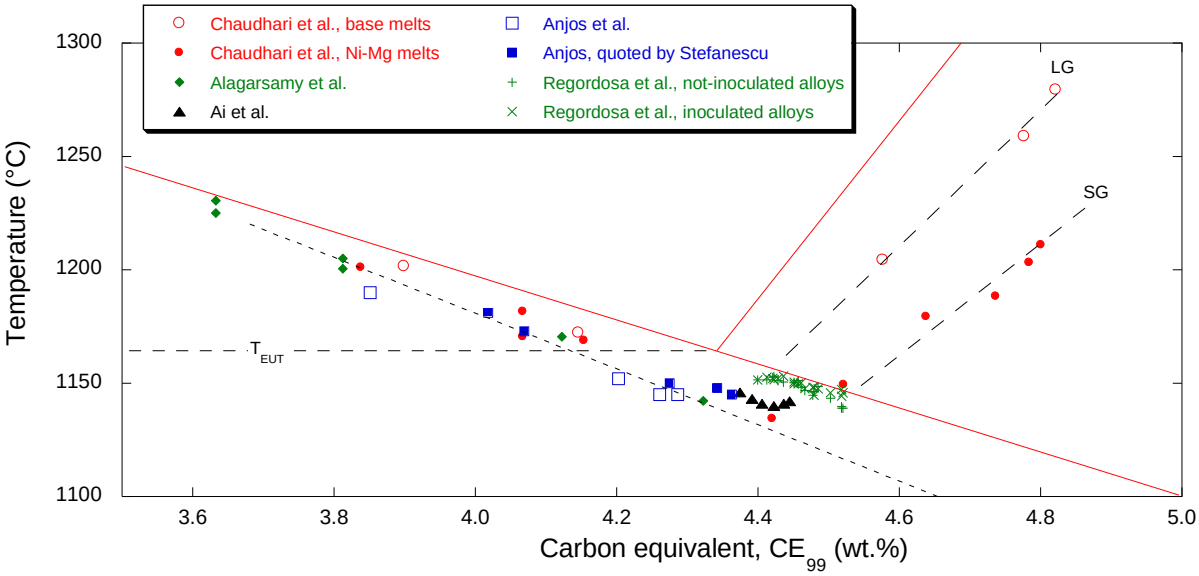

Figure 2. Symbols represent experimental temperatures for initiation of solidification from Chaudhari et al. [12], Alagarsamy et al. [17], Ai et al. [15], Anjos et al. [14], Anjos cited by Stefanescu [5] and Regordosa et al. [8]. The solid lines are the equilibrium liquidus for austenite (calculated with Equation 1) and for graphite (calculated with equation 2), and the short dashed line is the best fit through Moore's data according to Equation 9. The dashed lines labelled LG and SG go through graphite liquidus arrests from Chaudhari et al. for lamellar and spheroidal graphite precipitation, respectively.

In Figure 3, the dashed LG and SG lines of figure 2 have been changed to arrows following previous finding [6]. In fact, growth of primary spheroidal graphite of strongly hyper-eutectic alloys starts when the SG line is reached, and it has been shown that the solidification path of the alloys then more or less follows the SG arrow to hit the austenite liquidus at the temperature corresponding to the arrow end. Accordingly, the cooling curves of strongly hyper-eutectic alloys showed an arrest associated with the formation of austenite at the same temperature whatever was their CE value. It was considered that the same applies to lamellar graphite [6] and this is accepted here again by changing the dashed LG line in a dashed arrow that indicates the solidification path of strongly hyper-eutectic alloys during primary precipitation of lamellar graphite.

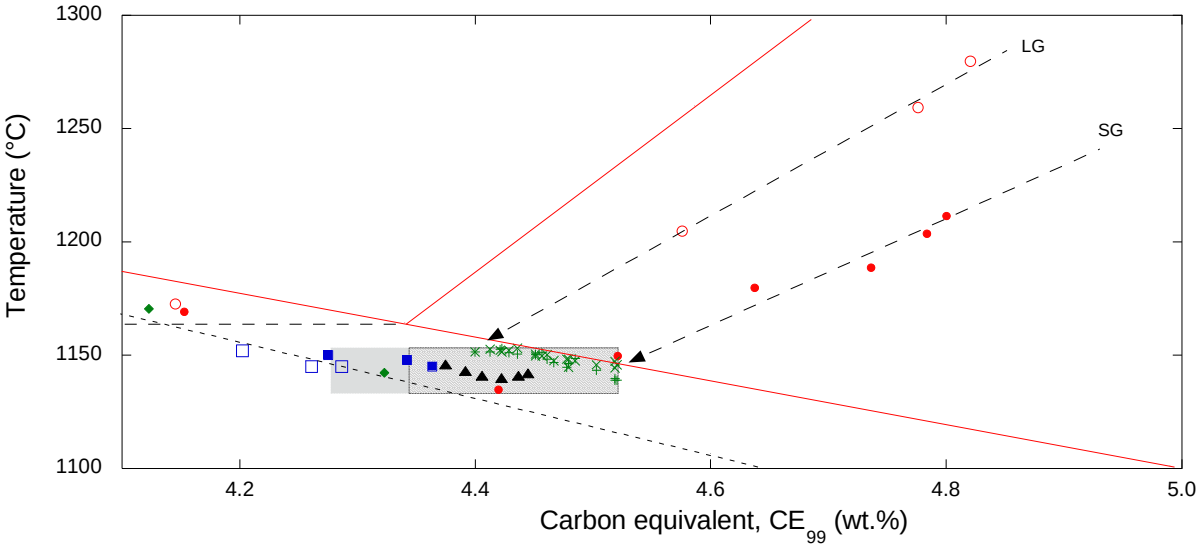

Figure 3. Zoom in the central part of Figure 2. The symbols are the same as in figure 2.

The narrow range of temperature for the start of solidification of near-eutectic alloys that was mentioned above is now exemplified with the hatched and greyed rectangle in figure 3. The hatched part of the rectangle is somehow similar to the one drawn in the figure 4 of Chaudhari et al. [12] which they defined as spanning CE values (calculated as $w_C+1/3 \cdot w_{Si}$) from the eutectic at 4.26 wt.% to 4.60 wt.% (as for the authors). In this range of composition, no arrest associated to primary graphite was recorded by thermal analysis [12]: solidification consisted in only a eutectic plateau for base melts, in an initiation arrest followed by a eutectic plateau for Ni-Mg treated melts. Chaudhari et al. labelled this initiation arrest as T_{EN}: it corresponds to the formation of austenite and was thus assumed to relate to the start of the eutectic reaction

as graphite was thought to have already appeared. However, T_{AL} and T_{EN} arrests are very similar being both related to the formation of austenite and the report by Chaudhari et al. showed how difficult it was for the authors to differentiate them. This can be understood as the amount of graphite that has precipitated when austenite forms can be quite small because the critical undercooling relative to the graphite liquidus indicated by the SG line has not been reached.

Because the T_{AL} and T_{EN} arrests are similarly due to formation of austenite, and because they are generally hardly differentiated, it could be proposed to use T_{LA} for both. However, there happen records where two successive limited arrests are observed before the eutectic plateau, in which cases it is obvious to call the first T_{LA} and the second T_{EN} [16].

Another example of cooling curves showing only a eutectic plateau or one arrest associated to austenite followed by a eutectic plateau was reported in the series of castings of mildly hypereutectic alloys by Regordosa et al. [8]. Figure 4 compares the cooling curves of the third casting (labelled C in the original paper) when cast in a plain cup (not-inoculated) and in a cup containing inoculant. The inoculated alloy solidified with one single eutectic plateau, as did all other inoculated alloys. For these alloys, the temperature for the onset of solidification was read at the slope change just before the eutectic plateau and was called T_{LA} though not associated with a separate arrest. In contrast, the alloy cast in the empty cup solidified in two steps, a short arrest associated with austenite formation followed by a eutectic plateau. Here also, the onset of solidification was read at the slope change indicating the start of the short arrest and denoted T_{LA} as well. Owing to the mildly hypereutectic nature of the alloys, the onset temperature should have been denoted T_{EN} according to Chaudhari et al. but the T_{LA} denomination was preferred as discussed above.

The fact that hypereutectic alloys can exhibit austenite dendrites has been known since works in the 1960s. This is true for irons with either lamellar or spheroidal graphite, though being much easier to evidence in these latter because of the higher eutectic undercooling that gives some more time for dendrites to grow. This seems to be accepted in Stefanescu's work [5] who states that "solidification morphology of the melt for composition above the eutectic point is highly dependent on the inoculation potential of the melt. If the melt has a low inoculation potential, it will still have hypoeutectic solidification morphology, although the CE is characteristic of eutectic or even hypereutectic composition." In agreement with this statement, the cooling curves of a mildly hypereutectic alloy may or not present a marked T_{LA} arrest as illustrated in Figure 4, and when this happens austenite dendrites are expected to show up in the microstructure.

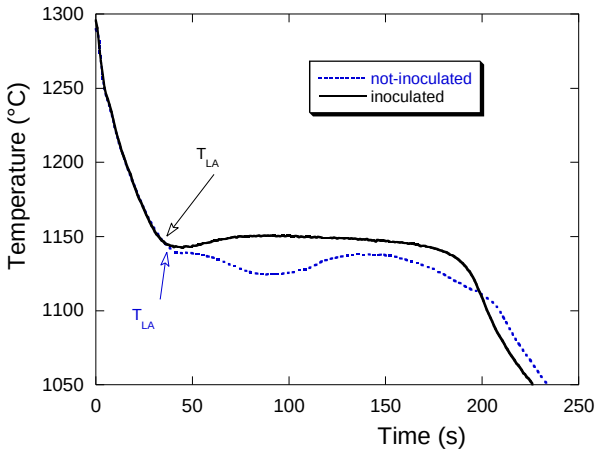

Figure 4. Cooling curves of inoculated and not-inoculated alloy C from the work by Regordosa et al. [8].

Revisiting thermal analysis results suggested the hatched area in Figure 3 should be extended to compositions lower than that corresponding to the eutectic [6, 18], this is illustrated with the greyed zone. In this area, growth undercooling of austenite is such that it grows at a temperature that is significantly below T_{EUT} and could possibly equal the growth temperature of the eutectic. For such near-eutectic hypo-eutectic alloys, the solidification front that grows inwards from the outer surface of the thermal analysis cup consists of austenite dendrites followed by a eutectic front. Depending on composition and inoculation, these fronts may grow apart, and a T_{LA} arrest will be recorded, or the dendrites can be engulfed within the eutectic front and only a eutectic plateau will appear on the cooling curve.

It was also shown in our previous work [6] that the boundary to the right of the hatched area corresponds to an undercooling with respect to the graphite liquidus that is high enough for simultaneous growth of graphite with austenite. This undercooling differs depending on the graphite shape, it is lower for lamellar graphite and then corresponds to the upper limit of the rectangle, and higher for spheroidal graphite when it corresponds to the lower limit of the rectangle. Accordingly, the boundary to the right of the rectangle in figure 3, that defines the upper limit for mildly hypereutectic cast irons, is valid for spheroidal graphite cast irons. For irons with lamellar graphite, this boundary is much closer to the stable eutectic and corresponds to the end of the LG arrow.

The schematic that was elaborated above for the description of the onset of solidification of mildly hypereutectic alloys is in full agreement with the short-cut by Chaudhari et al. [12] who stated that "the graphite liquidus and the eutectic initiation event tend to merge" in this composition range.

Discussion

This discussion deals with two features: 1. The interest of adding a kinetic term to CE to account for magnesium; 2. The possibilities of using CEL for hypereutectic alloys as function of the silicon content.

Lekakh et al. [4] and Stefanescu [5] have suggested adding a term to the expression of CE to account for the magnesium content of the cast irons and Stefanescu [5] used the literature data mentioned above to assess it. However, it remains unclear if this author was considering a kinetic term or an effect of magnesium on the equilibrium phase diagram. It has been shown in Appendix B that this latter possibility is totally excluded, as magnesium added at the level it is used for spheroidizing iron melts does not change to any significant level the equilibrium austenite and graphite liquidus. However, it is a simple matter to plot again the results in Figure 3 versus a "kinetic" CE, $CE_{KIN}=CE_{99}+m_{Mg}.w_{Mg}$, where m_{Mg} was set equal to the value of -1.05 selected by Stefanescu. Apart for a larger scattering of the results on hypo-eutectic alloys, it is seen with figure 5 that including the kinetic term associated with magnesium does not bring any further hint to the description of the results made above.

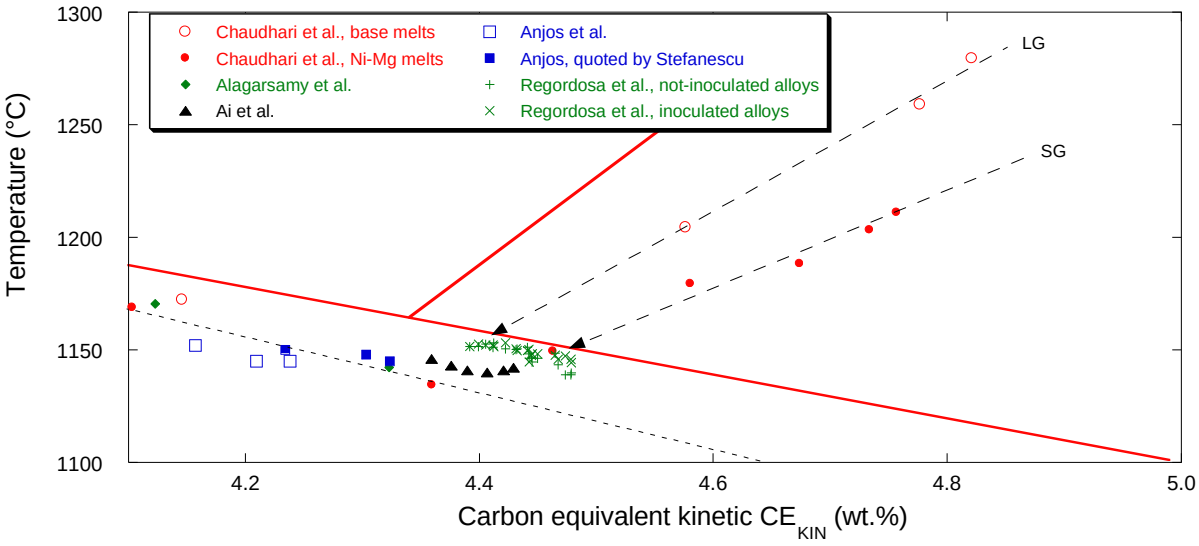

Figure 5. Same figure as Figure 3 but using CE_{KIN} instead of CE_{99} (see text).

As the alloys selected for figures 2, 3 and 5 have a silicon content in a limited range, they mostly differ by their carbon content. Accordingly, Stefanescu, in his Figure 12, plotted the liquidus values versus the carbon content for spheroidized alloys from Chaudhari et al. [12], Anjos (his table 7) and the not-inoculated alloys from Regordosa et al. [8]. A similar graph appears in figure 6 where the liquidus lines have been calculated as for the previous figures of the present work with the silicon content set at 2.45 wt.%. In addition, the results of inoculated alloys from Regordosa et al. were used instead of those of non-inoculated alloys, which does not change the characteristics of the graph because the results of inoculated and non-inoculated alloys are intermingled (see figure 2, 3 or 5). Following Stefanescu's work, the SG line suggests a carbon content at the eutectic at more than 3.7 wt.%, about 0.1 wt.% higher than the calculated equilibrium carbon content.

The reason for using data for inoculated alloys from Regordosa et al. in Figure 6 instead of the results for not-inoculated alloys as done by Stefanescu is that the cooling curves of all of these inoculated alloys showed only a eutectic plateau as already indicated in relation with figure 4, i.e., they all behaved as eutectic alloys. As seen in Figure 6, the loss in carbon content of the melt during the 8-hours holding was up to near 0.1 wt.% and it is thus concluded that their mode of solidification is not simply related to their position with respect to the eutectic point but accounts also for the decrease in magnesium. This stresses again the importance of the coupling between the possibility of graphite growth and the formation of

austenite in mildly hypereutectic alloys that is much better illustrated with the support of Figure 3 than that of Figure 6.

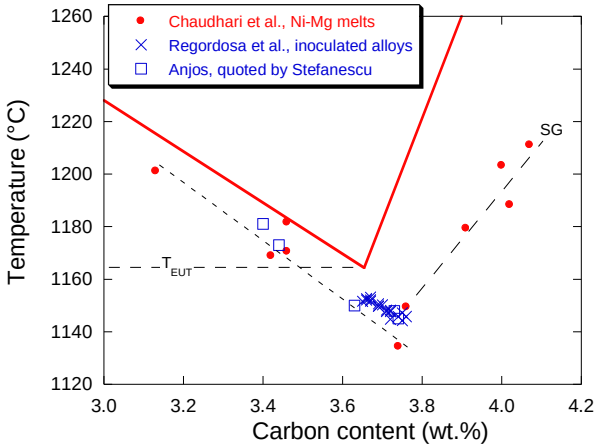

Figure 6. Plot of a selection of T_{LA} values of spheroidized melts as function of the carbon content. The solid lines are the austenite and graphite liquidus, the dashed SG line is the same as in figure 2 and the short dashed line corresponds to equation (9), all calculated at 2.45 wt.% Si.

The second part of the discussion concerns the possibility of determining CEL values of alloys that are hypereutectic according to the stable diagram. This principle goes back also to the 1960s and the use of tellurium for avoiding precipitation of graphite has been patented quite early [24]. Provided this condition is fulfilled, the upper limit in CEL determination is given by the location of the metastable eutectic that will replace the stable one and cannot be impeded. This has been already considered by Moore [2] who provided a projection of the two eutectic lines on the composition plane that is repeated here in figure 7. The technique can be “extended up to the kish point, i.e., the temperature at which free graphite forms and floats out of the molten cast iron as it cools” [24]. In practice, on-going work shows that it is hardly possible to totally impede graphite precipitation at silicon content higher than 3.5-4 wt.%.

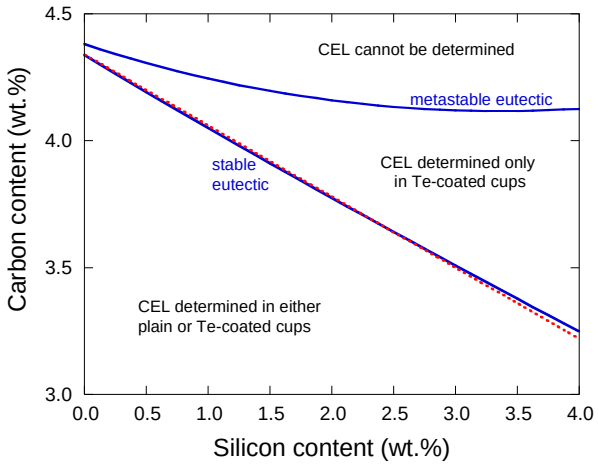

Figure 7. Composition domains for determination of CEL, after Moore [2]. Solid curves are the stable and metastable eutectic valleys plotted in the (w_C, w_{Si}) composition plane as calculated with the TCFE-8 database. The red dotted line is calculated according to Equation 5 and it is seen it is perfectly superimposed to the thermodynamic calculation for silicon contents lower than 3 wt.%.

Conclusion

For silicon cast irons with less than 3 wt.% silicon, the equilibrium CEL and CE can be expressed as two differing linear functions of composition. Using the equilibrium CEL_{99} to plot experimental austenite liquidus temperatures from standard thermal analysis gave a fairly good linear representation of the results for alloys with 1 to 3 wt.% silicon. The recourse to tellurium coated thermal analysis cups allowed extending this relation to CEL values close to that of the metastable eutectic. However, the experimental slope differs from the equilibrium one, indicating kinetic effects due to thermal transfer, melt processing and carbon content.

Analysis of the solidification onset of near eutectic to strongly hypereutectic alloys involving graphite, i.e., stable solidification, should be carried out for alloys with similar silicon contents because of the effect of this element on the eutectic temperature. Plotting the onset temperature as function of CE evidenced that near eutectic hypoeutectic alloys and mildly hypereutectic alloys start solidifying in a limited temperature range indicative of a coupling between austenite and eutectic growth. This temperature range corresponds also to a carbon content in the liquid that relates to an undercooling with respect to the graphite liquidus that is high enough for graphite to grow.

References

[1] M.D. Chaudhari, R.W. Heine, C.R. Loper, Potential applications of cooling curves in ductile iron process control. AFS Trans. 82, 379-386 (1974)

[2] A. Moore, Measurement of carbon equivalent liquidus values in hyper-eutectic flake-graphite irons. Foundry Trade J. 30, 885-890 (1971)

[3] A. Moore, Carbon equivalent of white cast irons. AFS Cast Metals Research J., 15-19 (1972)

[4] S. Lekakh, Technical Discussion Appendix, Comments on A. Regordosa, J. Sertucha, J. Ramon Olaizola, J. Lacaze article ‘‘When is a cast iron eutectic?’’. Inter Metalcast 16,119-131 (2021). https://doi.org/10. 1007/s40962-021-00587-7

[5] D.M. Stefanescu, Analysis of the rationale and accuracy of the use of carbon equivalent and thermal analysis in the quality control of cast iron. Int. J. Metalcasting 16, 1057–1078 (2022)

[6] M. J. Castro-Román, J. Lacaze, A. Regordosa, J. Sertucha, R. del Campo-Castro, Revisiting Thermal Analysis of Hypereutectic Spheroidal Graphite Cast Irons. Metall. Mater. Trans. A 51A, 6373-6386 (2020). https://doi.org/10.1007/s11661-020-06005-7

[7] M. Castro, M. Herrera, M.M. Cisneros, G. Lesoult, J. Lacaze, Simulation of thermal analysis applied to the description of the solidification of hypereutectic SG cast irons. Int. J. Cast Metals Research 11, 369-374 (1999)

[8] A. Regordosa, U. de la Torre, J. Sertucha, J. Lacaze, Quantitative analysis of the effect of inoculation and magnesium content on compacted graphite irons – Experimental approach. J. Mater. Process. Technol. 9, 11332-11343 (2020). https://doi.org/10.1016/j.jmrt.2020.08.008

[9] Thermocalc softwares and databases, https://thermocalc.com/products/

[10] J. Lacaze, J. Sertucha, M.J. Castro-Román, From atom scale to casting : A contemporary monograph on silicon cast irons microstructure, https://oatao.univ-toulouse.fr/26869/

[11] R.W. Heine, Liquidus and eutectic temperatures and solidification of white cast irons. AFS Trans. 85, 537-544 (1977)

[12] M.D. Chaudhari, R.W. Heine, C.R. Loper, Principles involved in the use of cooling curves in ductile iron process control. AFS Trans. 82, 431-440 (1974)

[13] G. Alonso, D.M. Stefanescu, R. Suarez et al., Kinetics of graphite expansion during the solidification of lamellar and spheroidal graphite iron. AFS Trans. 122, 237–248 (2014)

[14] V. Anjos, R. Deike, C.S. Ribeiro, The use of thermal analysis to predict the dendritic coherency point on nodular cast iron melts. Cienca & tecnologia dos Materiais 29, e27-e33 (2017)

[15] S. Ai, Z. Xu, Z. Liu et al., Evolution of inoculation thermal analysis and solidification morphology of compacted graphite iron. Kovove Mater. 59, 51–57 (2021) https://doi.org/10.4149/km2021151
[16] A. Regordosa, J. Sertucha, J.R. Olaizola, J. Lacaze, When is a cast iron eutectic? Int. J. Metalcasting 16, 119-131 (2022) https://doi.org/10.1007/s40962-021-00587-7
[17] A. Alagarsamy, F.W. Jacobs, G.R. Strong, R.W. Heine, Carbon equivalent vs. austenite liquidus: what is the correct relationship for cast irons? AFS Trans. 92, 871-880 (1984)
[18] A. Regordosa, J. Lacaze, J. Sertucha, M.J. Castro-Roman, U. de la Torre, O. Dezellus, Is thermal analysis able to provide carbon and silicon contents of cast irons? Int. J. Metalcasting, https://doi.org/10.1007/s40962-022-00799-5
[19] F. Mampaey, Modeling and experimental validation of austenite dendrite growth. AFS Trans. 106, 469-476 (1998)
[20] F. Mampaey,Application of austenite dendrite growth model to analyse liquidus temperature measurements in cups, AFS Trans. 106, 461-467 (1998)
[21] J.M. Frost, D.M. Stefanescu, Melt quality assessment of SG iron through computer-aided cooling curve analysis, AFS Trans. 100, 189-200 (1992)
[22] P.K. Basutkar, R.W. Heine, C.R. Loper, Effect of magnesium and cerium additions on the Fe-C-Si diagram. AFS Trans. 81, 336–340 (1973)
[23] K. Yamane, H. Yasuda, A. Sugiyama et al., Influence of Mg on solidification of hypereutectic cast iron: x-ray radiography study. Metall. Mater. Trans. A 46A, 4937–4946 (2015)
[24] W.T. Bourke, S. Harris, T.C. Muff, Method of producing an initial thermal arrest in the cooling curve of hypereutectic cast iron, US Patent 3,546,921, 1970

Appendix A.

Tables 1 and 2 list the data from Chaudhari et al. on base alloys (table 1) and on Ni-Mg spheroidized alloys (Table 2) [12]. This is the same data as selected by Stefanescu [5] with a couple of more results.

Table A1. Composition (wt.%) of base alloys, CEL_{99} and CE_{99} values (wt.%), and experimental liquidus temperature T_L (either austenite or graphite).

Alloy reference	Carbon content	Silicon content	CEL_{99}	CE_{99}	T_L (°C)
S2-1	2.71	1.64	3.10	3.17	1270.6
S15-1	3.02	1.40	3.35	3.41	1243.3
1101	2.80	2.84	3.47	3.60	1233.3
1203	3.16	2.64	3.78	3.90	1201.7
3201	3.53	2.20	4.05	4.15	1172.2
1301	3.74	2.46	4.32	4.43	
2201	3.84	2.63	4.46	4.58	1204.4
1401	4.06	2.56	4.66	4.78	1258.9
2402	4.11	2.54	4.71	4.82	1279.4

Table A2. Composition of Ni-Mg treated alloys, value of CEL_{99} and CE99 (wt.%) and experimental liquidus temperature T_L (either austenite or graphite).

Alloy reference	Carbon content	Silicon content	CEL_{99}	CE_{99}	T_L (°C)
S5-2	2.54	1.63	2.99	3.04	1291.1
S3-2	2.81	1.74	3.29	3.34	1263.3
S2-2	3.06	1.81	3.56	3.61	1232.2
1211	3.13	2.53	3.80	3.88	1201.1
3203	3.46	2.17	4.04	4.11	1170.6
1309	3.74	2.43	4.38	4.47	1134.4
2203	3.76	2.72	4.47	4.57	1149.4
2303	3.91	2.60	4.59	4.68	1179.4
1409	4.02	2.56	4.69	4.78	1188.3
2407	4.07	2.61	4.75	4.85	1211.1
3405	4.00	2.80	4.73	4.83	1203.3

Appendix B – Effect of magnesium on the equilibrium liquidus

Yamane et al. [23] investigated in situ using synchrotron X-ray tomography the solidification of two hyper-eutectic alloys, one with 0.002 wt.% residual Mg (3.69 C, 2.71 Si, 0.45 Mn, wt.%) and one spheroidized with 0.05 wt.% Mg (3.73 C, 2.57 Si, 0.45 Mn, wt.%). The CE_{99} value of both alloys is 4.45 wt.%. After melting of the alloys, the authors observed during cooling at 0.17°C/s that nucleation and growth of primary graphite proceeded in a temperature interval of about 20°C for the alloy without Mg while this temperature interval was limited to 3°C for the spheroidized alloy. The author mentioned that there could be two explanations to this effect of adding magnesium: 1. It inhibits graphite nucleation (or rather growth); 2. It affects phase equilibria. Yamane et al. disregarded the first possibility and investigated further the second one, concluding that 0.05 wt.% Mg depresses the graphite liquidus by 45°C. Such an effect means that the graphite liquidus depression is about 900°C/wt.% Mg which is more than significant and rather doubtful. In fact, the effect of Mg on the graphite liquidus may be estimated on the C-rich side of the C-Mg phase diagram and the slope is slightly lower than 30°C/wt.% Mg, i.e., 30 times lower than the value implied by Yamane's assumption. This conclusion was further substantiated by calculation performed with the TCFE-8 database of Thermocalc illustrated in Figure 8. This figure shows isopleth Fe-C sections at 2.5 wt.% Si with 0 and 0.06 wt.% Mg, and it is seen that they are superimposed (only the second digits in temperature are modified with the addition of Mg). On the contrary, the 45°C difference mentioned above is of the order of the shift between LG and SG lines in Figure 2 or 3, suggesting that the effect of Mg on growth of graphite was in fact the reason for the observations by Yamane et al.

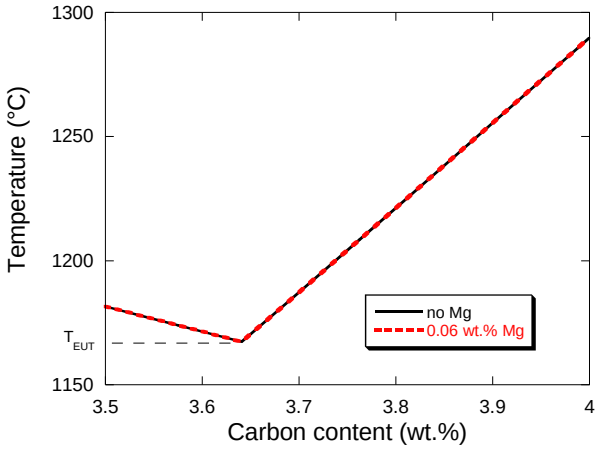

Figure 8. Isopleth Fe-C section at 2.5 wt.% Si calculated with no Mg and with 0.06 wt.% Mg using the TCFE-8 databank [9].